

Graph state engineering by phase modulation of the quantum optical frequency comb

Xuan Zhu,¹ Chun-Hung Chang,¹ Carlos González-Arciniegas,¹ Jacob Higgins,¹ Avi Pe'er,² and Olivier Pfister¹

¹*Department of Physics, University of Virginia, 382 McCormick Road, Charlottesville, VA 22903, USA*

²*Department of Physics and BINA Center of Nano-technology, Bar-Ilan University, 52900 Ramat-Gan, Israel*

(Dated: April 22, 2022)

The quantum optical frequency comb (QOFC) of a single optical parametric oscillator (OPO) is a scalable platform for quantum information as a generator of large size cluster states. We show that the phase modulation of the QOFCs emitted by an OPO is a powerful graph engineering technique that can increase the topological dimension of the generated cluster state, from zero (independent EPR pairs) to one (linear cluster state), and from one to two (square-lattice cluster state), thereby allowing the creation and tailoring of universal quantum computing resources. This concept is highly compatible with integrated photonics.

I. INTRODUCTION

The coming of age of quantum engineering is required for realistic (especially, field-compatible) quantum information devices to be conceived in earnest. Quantum photonics offers the perspective of marrying the fundamental advances of quantum optics and quantum information with the constantly evolving technology of integrated photonics.

Just as the transition from AM to FM heralded a new age for radio broadcasting, the spectral encoding of quantum information is a promising avenue [1]. In particular, the encoding of quantum information in the emission spectrum of a single optical parametric oscillator (OPO), a.k.a. the quantum optical frequency comb (QOFC), presents a compelling array of possibilities. When quantum information is encoded in the quantum electromagnetic fields, or qumodes, associated with respective OPO cavity modes, massively multipartite entangled states can be generated [2–4]. The qumode encoding makes use of the continuous variables that are the quadrature eigenstates of the quantum electromagnetic field (analogues of the position and momentum eigenstates of the quantum harmonic oscillator), the entangled qumode states being multimode squeezed states [1]. Note that such field-based, qumode encodings have also been realized in the temporal domain [5–7]. In both the frequency and time domain aforementioned works, the generated multipartite entanglement was of the cluster state type. Cluster states are a key resource for measurement-based, namely one-way, quantum computing, a variant of quantum computing which is also universal and was first formulated for qubits [8, 9] and then for qumodes [10, 11]. Scalable cluster states constitute the principal component of the required hardware for quantum computing and qumode-encoded cluster states therefore hold great promise for the practical implementation of one-way quantum computing.

It is interesting to note also that a parallel line of effort on quantum information in the QOFC had focused on photon pair generation in frequency bins in integrated optics [12, 13]. While this makes use of the wealth of existing classical results for frequency combs on chip, the

current state of the art for losses in integrated optics components mandates the quantum redeeming postselection process of coincidence detection, which places an exponential limitation on scalability, even though a polynomial scalability gain may still be obtained from using frequency-bin-encoded qudits rather than qubits. In order to enable scalability in integrated optics, it will be crucial to bring losses down to the fault-tolerant level, at which quantum error correction can be employed [14, 15].

Spectral qumode encoding in free-space optics isn't as limited by losses and doesn't require postselection as a result. Multipartite entanglement over very large scales has been obtained by (i), concurrent [16] nonlinear interactions [2]; (ii), interference of two distinct, offset two-mode-squeezed QOFCs yielding long “quantum-wire” cluster entangled states [3], a process that was generalized to, (iii), a proposal to generate hypercubic cluster states of arbitrary topological dimension [17]; (iv), a hybrid time-frequency encoding approach can also be used [18]; finally, (v), a QOFC has been demonstrated in a synchronously pumped OPO [4] for which pump spectral engineering could also be used [19].

In this paper, we explore a different approach that consists in applying phase modulation to a QOFC at frequencies multiple of its qumode spacing. The phase modulator can be considered and modeled as a frequency-domain beamsplitter [20] and applying it to the periodic QOFC field structure eschews contamination by vacuum modes, as illustrated in Fig.1. We will consider the bipartite-wise entangled QOFC of a single OPO emitting multiple two-mode squeezed mode pairs from a single monochromatic pump field. The phase modulation will then interfere different two-mode-squeezed (TMS) field pairs in much the same way as in cases (ii,iii) above. As we will show, this very simple experimental setup of an OPO followed by an electro-optic modulator (EOM) provides a rich array of possibilities for quantum state engineering, including the possibility to generate square-lattice cluster states which are key resources for universal measurement-based quantum computing.

In Section II, we introduce the fundamentals of the theory of Gaussian graph states and their derivation for squeezing and phase modulation operations. In Sec-

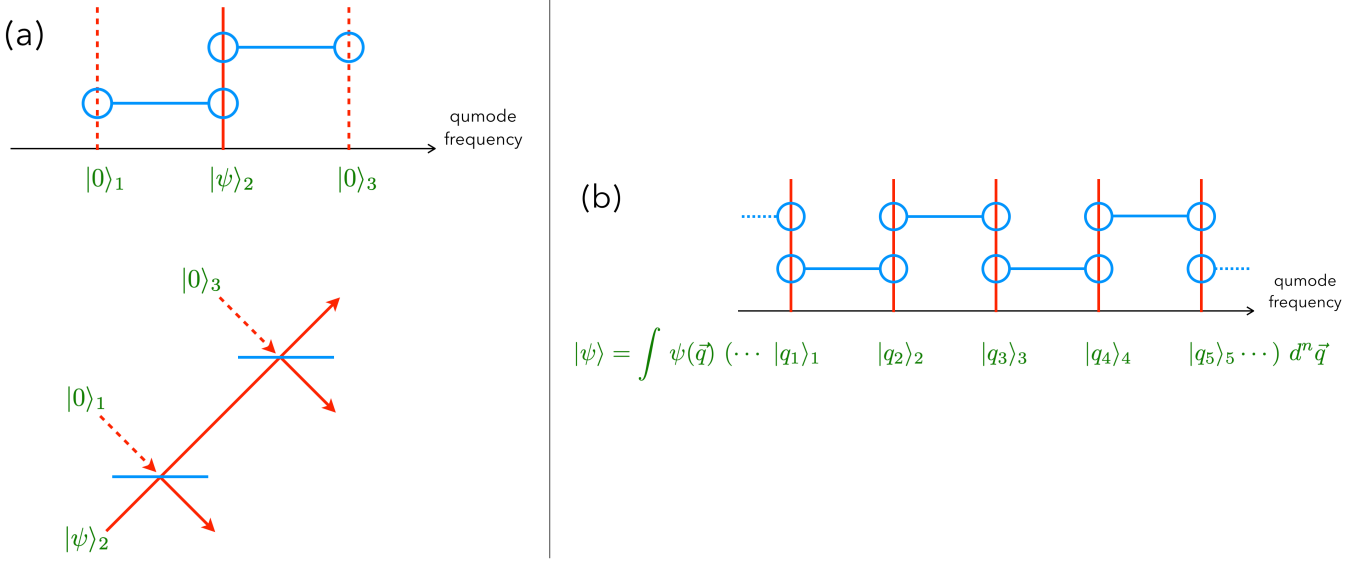


FIG. 1. Principle of graph state engineering by phase modulation, whose action, here in the limit of small modulation index (first-order sidebands only), is equivalent to beamsplitter mode-coupling, as per the blue lines, of the initial quantum states, in green; (a), top, “classical” phase modulation, in which vacuum sidebands couple in with the initial quantum state $|\psi\rangle$; (a), bottom, spatial analogue; (b), the phase modulation of the QOFC at the mode frequency spacing has no vacuum input and realizes a complex unitary operation on initial state $|\psi\rangle$.

tion III, we present our theoretical results for the graph states generated under various experimental conditions involving phase modulation.

II. THEORY REMINDERS

A. Graph state definition

The exact analogues of qubit cluster [8] or graph [21] states for continuous variable (CV) quantum information are well defined [1, 10, 22]. (Note that the terms “cluster state” and “graph state” are often used somewhat interchangeably in the literature. We adopt the term “graph” for arbitrary graph states and “cluster” for the specific graphs that are sparse enough to be relevant to measurement-based quantum computing [23–25].) A qubit graph state is canonically defined as graph vertices j denoting qubits in state $|+\rangle_j = (|0\rangle_j + |1\rangle_j)/\sqrt{2}$ and graph edges (j, k) denoting controlled Z gates CZ_{jk} . For qumodes in the unphysical limit of infinite squeezing, a graph state is composed of vertices j denoting field phase-quadrature eigenstates $|p=0\rangle_j$ (of $P = (a - a^\dagger)/(i\sqrt{2})$, a being the photon annihilation operator) and of edges (j, k) denoting the quantum non-demolition [26] controlled phase interaction $\exp(iQ_j Q_k)$, where $Q = (a + a^\dagger)/\sqrt{2}$ is the field amplitude quadrature. Realistic qumodes cannot be infinitely squeezed but squeezed states remain an arbitrarily good approximation to CVQI, and fault tolerance was proven to exist for finitely squeezed states [14]. In this case, a graph state

is composed of vertices j denoting phase-squeezed states, obtained from vacuum by use of the squeezing operator

$$|0, r\rangle_j = S(r)|0\rangle_j = e^{\frac{r}{2}(a^{\dagger 2} - a^2)}|0\rangle_j, \quad (1)$$

where r is the squeezing parameter. The graph edges (j, k) still denote the controlled phase shift gate $\exp(iQ_j Q_k)$.

As we already mentioned, the squeezing in the QOFC will be directly generated, in our model, by an optical parametric amplifier (OPA), i.e., an OPO below threshold. The squeezing Hamiltonian of this system is

$$H = i\hbar \frac{r}{2\tau} \sum_{j=1}^N \sum_{k=1}^N (2 - \delta_{jk}) G_{jk} a_j^\dagger a_k^\dagger + \text{H.c.}, \quad (2)$$

where r is the squeezing parameter, τ is the interaction time, and a_j and a_k are the annihilation operators of qumodes j and k , respectively. The $N \times N$ matrix \mathbf{G} is the adjacency matrix [27] of the \mathcal{H} -graph [28]. If the pump is monochromatic, the \mathbf{G} matrix has Hankel form, e.g., for $\omega_p = \omega_1 + \omega_N$,

$$\mathbf{G} = \begin{pmatrix} 0 & \cdots & 0 & 1 \\ \vdots & \ddots & \ddots & 0 \\ 0 & \ddots & \ddots & \vdots \\ 1 & 0 & \cdots & 0 \end{pmatrix}. \quad (3)$$

There exists a mathematical relation between adjacency matrix \mathbf{G} and the graph formalism for Gaussian states [29]. In the following, we outline its salient points as well as the formal steps of the derivation of a Gaussian graph state. Readers interested in more details and complete proofs should consult Ref. 29.

The finitely squeezed CV graph state generated by Eqs. (2) & (3) (and any Gaussian state, in general) can be described by a unique complex adjacency matrix

$$\mathbf{Z} = \mathbf{V} + i\mathbf{U} = ie^{-2r}\mathbf{G} \quad (4)$$

where \mathbf{V} and \mathbf{U} are both real symmetric matrices and \mathbf{U} is also positive definite. In the ideal case ($r \rightarrow \infty$), $\mathbf{U} = 0$ and \mathbf{V} is the real adjacency matrix—to local unitaries left, which cannot change entanglement—of the graph state whose Weyl-Heisenberg stabilizer group is generated by

$$X_j \bigotimes_{k \in \mathcal{N}_j} Z_k \equiv e^{-i(P_j - \mathbf{V}_{jk} Q_k)}, \quad (5)$$

for each vertex j , \mathcal{N}_j being the graph neighborhood of j . While the graph state is, by definition, an eigenstate with eigenvalue one of the stabilizer operator on the left-hand side of Eq. (5), it is also an eigenstate with eigenvalue zero of the nullifier operator $P_j - \mathbf{V}_{jk} Q_k$ on the right-hand side of Eq. (5). In the case of finite squeezing parameter r , matrix \mathbf{U} will describe the deviation from the ideal graph due to residual quantum noise and we can just require that $\text{Tr}[\mathbf{U}] \rightarrow 0$ (typically $\sim e^{-2r}$) since \mathbf{U} is real symmetric and positive definite.

In the following, we will call \mathbf{V} the adjacency matrix and \mathbf{U} the error matrix of the graph.

Formally, the system of nullifiers of any Gaussian state can be written in matrix form

$$\mathbf{P} - \mathbf{Z}\mathbf{Q} = 0. \quad (6)$$

and also verifies

$$\text{cov}[\mathbf{P} - \mathbf{Z}\mathbf{Q}] = \mathbf{U}. \quad (7)$$

If we are interested in that Gaussian state also being a valid approximation of a graph state, we shall seek nullifiers of the form $\mathbf{P} - \mathbf{V}\mathbf{Q}$ such that

$$\text{cov}[\mathbf{P} - \mathbf{V}\mathbf{Q}] = \frac{1}{2}\mathbf{U} \quad (8)$$

$$\text{Tr}[\mathbf{U}] \rightarrow 0. \quad (9)$$

As pointed out earlier, the matrix \mathbf{U} can be thought of as the deviation from an ideal graph state.

B. Graph derivation

We make use of the Heisenberg picture to derive the nullifiers of the state and obtain \mathbf{Z} . Then we assess if it corresponds to a valid graph state, if $\text{Tr}[\mathbf{U}] \rightarrow 0$. The system of Heisenberg equations for the Hamiltonian of Eq. (2) can be written

$$\frac{d\mathbf{x}}{dt} = \frac{r}{\tau}\mathbf{G}\mathbf{x}, \quad (10)$$

where we posed $\mathbf{x} = (\mathbf{Q}, \mathbf{P})^T$, $\mathbf{Q} = (Q_1, \dots, Q_N)^T$, and $\mathbf{P} = (P_1, \dots, P_N)^T$. Equation (10) can be solved by diagonalizing $\mathbf{G} = \mathbf{R}\mathbf{G}_{\text{diag}}\mathbf{R}^{-1}$, yielding solution

$$\mathbf{x}(\tau) = \mathbf{S}\mathbf{x}(0), \quad (11)$$

where the symplectic matrix \mathbf{S} is given by

$$\mathbf{S} = \mathbf{R}e^{r\mathbf{G}_{\text{diag}}}\mathbf{R}^{-1}. \quad (12)$$

Note that, in a sequence of unitary operations, the symplectic matrix ordering is that of the Schrödinger picture

$$\mathbf{x}' = \mathbf{S}_n\mathbf{S}_{n-1} \cdots \mathbf{S}_1\mathbf{x} = \mathbf{S}\mathbf{x}. \quad (13)$$

Once the symplectic matrix \mathbf{S} of the system is obtained, The covariance matrix $\mathbf{\Sigma}$, which contains all information about a Gaussian state, can be derived as

$$\mathbf{\Sigma} = \frac{1}{2}\mathbf{S}\mathbf{S}^T, \quad (14)$$

and an important property of the covariance matrix is that it is related to the complex adjacency matrix \mathbf{Z} by

$$\mathbf{\Sigma} = \frac{1}{2} \begin{pmatrix} \mathbf{U}^{-1} & \mathbf{U}^{-1}\mathbf{V} \\ \mathbf{V}\mathbf{U}^{-1} & \mathbf{U} + \mathbf{V}\mathbf{U}^{-1}\mathbf{V} \end{pmatrix}, \quad (15)$$

where the block structure corresponds to the definition $\mathbf{x} = (\mathbf{Q}, \mathbf{P})^T$. This yields the graph \mathbf{V} if the error matrix \mathbf{U} is well behaved, i.e., verifies Eq. (9) in the limit of infinite squeezing.

An allowable strategy for modifying \mathbf{U} so its limit vanishes is to apply *local* operations to qumodes—optical phase shifts by $\pi/2$ [29]—since these cannot change the state separability, i.e., its entanglement.

Finally, we recall a direct rule for graph evolution under a symplectic transformation. We can always write the total symplectic matrix in the form:

$$\mathbf{S} = \begin{pmatrix} \mathbf{A} & \mathbf{B} \\ \mathbf{C} & \mathbf{D} \end{pmatrix}, \quad (16)$$

where the blocks follow the $\mathbf{x} = (\mathbf{Q}, \mathbf{P})^T$ structure. The Gaussian pure state evolution from an initial complex graph \mathbf{Z} to a new one \mathbf{Z}' under this operation is expressed by a Möbius transformation [29]

$$\mathbf{Z}' = (\mathbf{C} + \mathbf{D}\mathbf{Z})(\mathbf{A} + \mathbf{B}\mathbf{Z})^{-1}. \quad (17)$$

C. Symplectic matrix for phase modulation

The process of EOM phase modulation is modeled by a nonlinear interaction between two optical fields a_j and $a_{j+\Omega}$, at two frequencies differing by the modulation frequency $\Omega \in \mathbb{N}$, expressed in units of the OPO free spectral range (FSR), and the radio frequency field $a_R = \alpha e^{-i\phi}$, $\alpha \geq 0$, at the modulation frequency, which is assumed classical and unchanged (neither depleted nor amplified). Under these conditions, it is straightforward

to show that the effective Hamiltonian of this interaction has a beamsplitter form [20]

$$H = \hbar \frac{\alpha}{\tau} e^{-i\phi} \sum_{j=-\infty}^{\infty} a_j a_{j+\Omega}^{\dagger} + \text{H.c.}, \quad (18)$$

where τ is the interaction time. This yields the Heisenberg equations

$$\frac{da_j}{dt} = -i \frac{\alpha}{\tau} (e^{-i\phi} a_{j-\Omega} + e^{i\phi} a_{j+\Omega}) \quad (19)$$

whose solution

$$\begin{pmatrix} a'_1 \\ a'_2 \\ \vdots \\ a'_N \end{pmatrix} = \mathbf{M} \begin{pmatrix} a_1 \\ a_2 \\ \vdots \\ a_N \end{pmatrix} \quad (20)$$

is found by diagonalizing Töplitz matrices, as is clear from Eq. (19) for $\Omega = 1$. This still applies for $\Omega > 1$ because the matrix of the equation system Eq. (19) can always be block-diagonalized into Töplitz blocks. Using the eigenvalues and eigenvectors of Töplitz matrices [30], we find, for $\Omega = 1$,

$$M_{jk} = \frac{2}{N+1} \sum_{m=1}^N i^{j-k} \sin \frac{j m \pi}{N+1} \sin \frac{k m \pi}{N+1} \times \exp \left(i 2 \alpha \cos \frac{m \pi}{N+1} \right) \quad (21)$$

$$M_{jk} = J_{k-j}(2\alpha) - (-1)^j J_{k+j}(2\alpha) \quad (22)$$

where $J_{k\pm j}(2\alpha)$ are the Bessel functions of the first kind, which describe the phase modulation spectrum generated from a single initial mode in a coherent state, a result that was obtained by Capmany and Fernández-Pousa's model using the Hamiltonian of Eq. (18) [20]. From now on, we define the modulation index $m = 2\alpha$, which is the usual parameter convention for phase modulation. For $\Omega > 1$, we can get a similar result by block-diagonalizing \mathbf{M} into Töplitz blocks.

Figure 2 displays numerical calculations of the \mathbf{M} matrix for $\Omega=1$ and with respective modulation depths and indices $m=0.2$ [Fig.2(a)] and $m=1$ [Fig.2(b)]. Comparing Fig.2(a) and Fig.2(b), we see that a larger α, m yields, as expected, more modulation sidebands, and therefore nonzero elements extending farther away from the main diagonal.

The definition of the symplectic matrix \mathbf{S} that we'll use applies to the quadrature vector $\mathbf{x} = (\mathbf{Q}, \mathbf{P})^T$. The matrices \mathbf{S} and \mathbf{M} are then related by

$$\mathbf{S} = \begin{pmatrix} \mathbf{A} & \mathbf{B} \\ \mathbf{C} & \mathbf{D} \end{pmatrix} \equiv \begin{pmatrix} \text{Re}[\mathbf{M}] & i \text{Im}[\mathbf{M}] \\ -i \text{Im}[\mathbf{M}] & \text{Re}[\mathbf{M}] \end{pmatrix}. \quad (23)$$

D. Finite squeezing and weighted graph states: graph trimming

Before we turn to the full graph state derivations and assess what phase modulation brings to quantum state

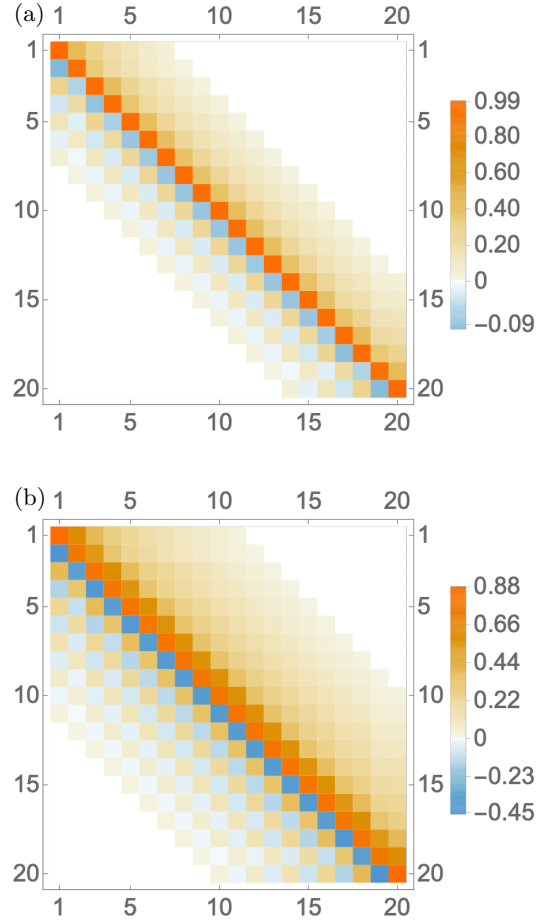


FIG. 2. EOM M-matrix numerical plot. (a) EOM modulation frequency $\Omega = 1$ FSR, $m = 0.2$. (b) EOM modulation frequency $\Omega = 1$ FSR, $m = 1$.

engineering in the QOFC, we need to examine the effect of finite squeezing on weighted graph states. Indeed, it appears highly likely from a cursory examination of Fig.2 that the effect of phase modulation will range in intensity from one qumode to another, depending, for example, on the modulation depth α , and also on the modulation frequency Ω . An important question is thus how finite squeezing affects the quantum correlations (graph edges) that are experimentally observable.

1. Example: a two-mode cluster state

We first take the simplest nontrivial example of the two-mode graph/cluster state, which also happens to be a general enough one.

In the limit of infinite squeezing, an isolated qumode 1 has, by definition, nullifier P_1 . The exact nullifier of qumode 1 in a single-mode squeezed (SMS) state of squeezing parameter r_1 is

$$\mathcal{N}_{s1} = S_1(r_1) a_1 S_1^\dagger(r_1) = P_1 - i e^{-2r_1} Q_1 \quad (24)$$

Two such phase-squeezed qumodes coupled by gate $C_Z = \exp(i\varepsilon Q_1 Q_2)$ form a Gaussian cluster state of nullifiers

$$\mathcal{N}_1 = C_Z \mathcal{N}_{s1} C_Z^\dagger = P_1 - i e^{-2r_1} Q_1 + \varepsilon Q_2 \quad (25)$$

$$\mathcal{N}_2 = C_Z \mathcal{N}_{s2} C_Z^\dagger = P_2 - i e^{-2r_2} Q_2 + \varepsilon Q_1. \quad (26)$$

We now ask the following question: if we wrongly assume qumode is isolated when it is, in fact, linked to qumode 2 by a graph edge whose weight ε is small: how large can ε be before it is detectable?

To answer this question, we must first relate it to the actual physical measurements we can make on qumode 1. Note that nullifiers in Eqs. (24-26) are not Hermitian, being derived from the annihilation operator [29]. We thus consider the measurement of quadrature P_1 , typically done by homodyne detection. In the case of an infinitely squeezed, truly isolated qumode 1, P_1 is the nullifier and thus has zero variance,

$$(\Delta P_1)^2 = {}_1\langle p=0 | P_1^2 | p=0 \rangle_1 = 0. \quad (27)$$

In the case of a finitely squeezed qumode 1, we have the well known result

$$(\Delta P_1)^2 = {}_1\langle 0 | S_1(r_1)^\dagger P_1^2 S_1(r_1) | 0 \rangle_1 = \frac{1}{2} e^{-2r_1}, \quad (28)$$

where the states are now vacuum ones. This indicates that P_1 is still the “best” observable to measure as it has the lowest noise. We now assume qumode 1 has a C_Z graph edge of weight ε with qumode 2 (squeezed by r_2), we have

$$(\Delta P_1)^2 = {}_{12}\langle 00 | S_2^\dagger S_1^\dagger C_Z^\dagger P_1^2 C_Z S_1 S_2 | 00 \rangle_{12} \quad (29)$$

$$= {}_{12}\langle 00 | (P_1 e^{-2r_1} - \varepsilon Q_2 e^{2r_2})^2 | 00 \rangle_{12} \quad (30)$$

$$= \frac{1}{2} e^{-2r_1} [1 + \varepsilon^2 e^{2(r_1+r_2)}]. \quad (31)$$

Comparing Eqs. (28) & (31), we deduce the condition for neglecting a graph edge of weight ε :

$$\varepsilon \ll \varepsilon_{\min} = e^{-(r_1+r_2)} \quad (32)$$

where ε_{\min} is basically the value at which the quantum noise is raised by 3 dB on a single qumode quadrature measurement.

2. General approach for multipartite graphs

An equivalent but more general approach, which we can use for any graph state, is to extensively use the formalism of Gaussian graphical calculus [29] and, in particular, Eq. (8). The procedure is the following: we define a “trimmed” version of the original graph $\mathbf{Z} = \mathbf{V} + i\mathbf{U}$ (for which we have $\text{Tr}[\mathbf{U}] \rightarrow 0$) by truncating matrix \mathbf{V} to \mathbf{V}_{tr} , i.e., replacing all elements V_{jk} smaller than a threshold value ε_{\min} with $V_{trjk} = 0$. This yields a new graph error matrix

$$\mathbf{U}_{\text{tr}} = 2\text{cov}[\mathbf{P} - \mathbf{V}_{\text{tr}}\mathbf{Q}], \quad (33)$$

which, in the previous two-mode case, is

$$\mathbf{U}_{\text{tr}} = \begin{pmatrix} e^{-2r_1} [1 + \varepsilon^2 e^{2(r_1+r_2)}] & 0 \\ 0 & e^{-2r_2} [1 + \varepsilon^2 e^{2(r_1+r_2)}] \end{pmatrix} \quad (34)$$

and the general condition for $\text{Tr}[\mathbf{U}_{\text{tr}}] \rightarrow 0$ becomes

$$\varepsilon \ll e^{-(r_1+r_2)}, \quad (35)$$

which is identical to Eq. (32) since $\mathbf{V}_{\text{tr}} = \mathbf{0}$ here.

Note that, in the case of a QOFC emitted by a single OPO, it's relatively straightforward to ensure that the squeezing parameter be the same for all TMS pairs, by judicious engineering of the quasimatched nonlinear material in the OPO [31].

III. GRAPH STATE ENGINEERING IN THE QOFC

We now investigate quantum state engineering by phase modulation of the QOFC. Several experimental configurations are considered, involving one or several QOFCs—up to four can be emitted by a single ring OPO using different polarizations and counterpropagating modes—as well as EOMs and interference.

A. Generation of 1D graph states by phase modulation of a single QOFC

1. Experimental configuration

The first case we study is the simplest, depicted in Fig.3: a polarization degenerate OPO is pumped at a

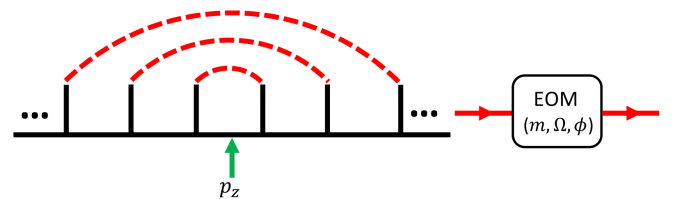


FIG. 3. Phase modulation of a single QOFC. An OPO with a single pump frequency, whose half is denoted by the green arrow, creates TMS qumode pairs as indicated by the red dashed lines. An EOM applies phase modulation with index m , frequency Ω , and phase ϕ (irrelevant in this case).

single frequency ω_p such that frequency $\omega_p/2$ is set exactly halfway between 2 OPO mode frequencies (usually by a phaselock loop [2, 3]). This generates independent “EPR pairs” of qumodes in two-mode-squeezed (TMS) states [32, 33], Fig.3, left. While entanglement scalability is already present in this OPO, it manifests itself as the scaling of the number of copies of a bipartite entangled state, rather than as the scaling of the size of a

multipartite state. Phase modulation by the EOM of the OPO QOFC will change that. The EOM frequency is set to $\Omega = 1$ in this case, with $m = 0.2$.

2. Graph derivation

The graph derivation proceeds as follows. First, we derive the EPR graph \mathbf{Z}_o from Eq. (4) and the OPA Hamiltonian, Eq. (2). Unsurprisingly, the graph is a set of disconnected qumode pairs, each pair containing an edge [29]. The action of the EOM can then be calculated by applying the Möbius rule, Eq. (17), using the symplectic matrix \mathbf{S} for phase modulation, Eq. (23), to obtain the final matrix $\mathbf{Z} = \mathbf{V} + i\mathbf{U}$.

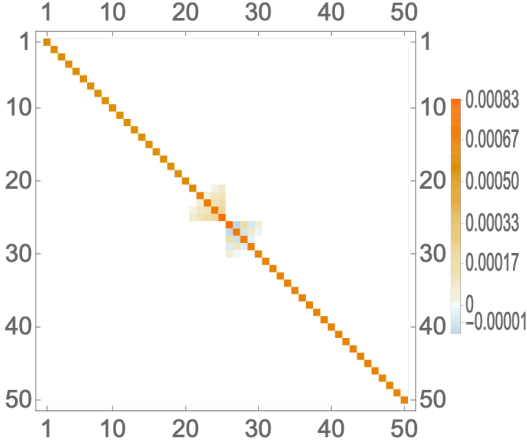


FIG. 4. Error matrix \mathbf{U} of a phase-modulated $N = 50$ QOFC with $(r, m, \Omega) = (1, 0.2, 1)$.

In order to assess whether \mathbf{V} is a valid graph adjacency matrix, we need to examine $\text{Tr}[\mathbf{U}]$ and confirm that $\text{Tr}[\mathbf{U}] \rightarrow 0$. As was mentioned above, the minimization of $\text{Tr}[\mathbf{U}]$ can be performed by applying local phase space rotations by $\frac{\pi}{2}$ to individual qumodes, which cannot modify the entanglement. Finding an algorithm to carry out this task is still an open question [29]. Here, we make use of the symmetry of the system, where a permutation symmetry can be found for qumodes symmetrically placed away from the pump's half-frequency, which therefore belong to the same EPR pair. Heeding this, we chose to apply the phase shifts (which are rotations in quantum phase space and therefore exchange Q and P —to a sign left, of course—and can thus be thought of as Fourier transforms of qumodes) to the first half of the N qumode set. This choice does lead to the desired result, see Fig.4.

Having established its validity, we can now turn to the graph adjacency matrix \mathbf{V} , shown in Fig.5. This adjacency matrix is that of a bicolored graph because it's block non-diagonal, which means that qumodes 1–25 are not coupled together (no diagonal block) and are only coupled to qumodes 26–50, which are also not coupled

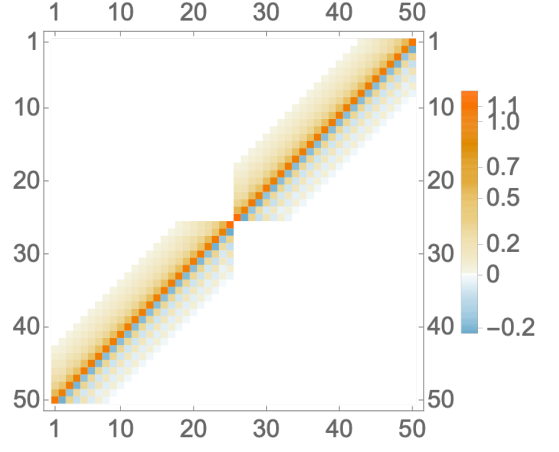


FIG. 5. Adjacency matrix \mathbf{V} of a phase-modulated $N = 50$ QOFC with $(r, m, \Omega) = (1, 0.2, 1)$. Values below 10^{-10} were not plotted.

together. The corresponding graph is depicted in Fig.6.

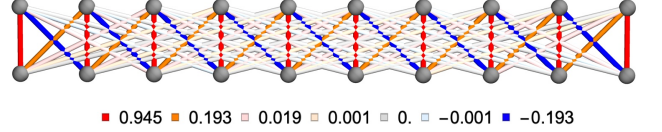


FIG. 6. Quantum graph corresponding to the \mathbf{V} matrix of Fig.5, here given for 20 qumodes only, for clarity. The half frequency of the pump is between modes 10 and 11.

3. Graph trimming

The edge weights (elements of \mathbf{V}) decrease relatively fast away from the main skew diagonal in Fig.5, with $V_{143} \sim 10^{-10}$ and $V_{126} \sim 10^{-40}$. Given this gradient of edge weights, we now ask the question of what part of the graph is actually detectable experimentally. We apply the procedure presented in Section IID to obtain the relevant threshold value ε_{\min} for a given squeezing level, as depicted on Fig.7. In this figure, the ordinate being the deviation, calculated from \mathbf{U} , to the graph state described by \mathbf{V} , we immediately see that truncation doesn't change the error for low enough values of ε_{\min} , the error staying essentially at the squeezing level. (Note that here we actually have $\text{Tr}[\mathbf{U}] \sim N \text{sech}(2r)$, rather than $N \exp(-2r)$; while both expressions admit the same limit for large squeezing, they do differ at low r . The former expression is, however, consistent with the analytic expression of the graph of a TMS state [29].) As ε_{\min} increases, the error rises because we are trimming graph edges which are now detectable by quadrature measurements in the laboratory. Higher values of squeezing mandate lower ε_{\min} : for example, $\varepsilon_{\min} = 10^{-1}$ clearly raises the error for squeezing > 10 dB (Fig.7). Any value of ε_{\min} above 1 should, of course, be nonsensical as the

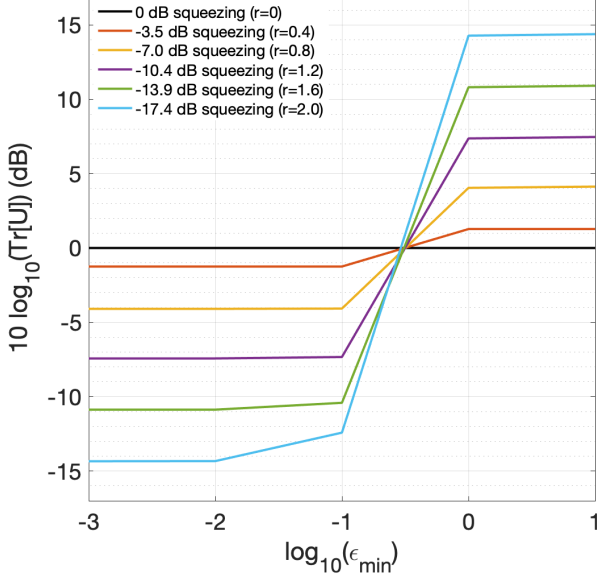


FIG. 7. Trimmed graph error versus truncation threshold for the graph of Fig.6, for $m = 0.2$.

graph is ultimately destroyed and the computed error rises sharply in confirmation of this.

Setting $\epsilon_{\min} = 0.1$ is valid for squeezing levels up to 10 dB—and 10 dB of squeezing has been shown to be enough [15] to ensure fault-tolerant quantum computing using the Gottesman-Kitaev-Preskill encoding [14]—and we obtain the trimmed graph displayed in Fig.8. This

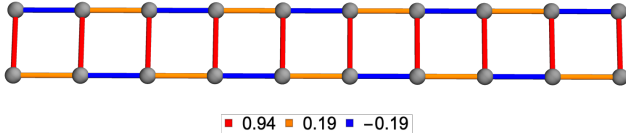


FIG. 8. Partial view of the bulk structure of the trimmed graph of Fig.6, for $\epsilon_{\min} = 0.1$. Edges weights: red, 0.94; blue, -0.19; orange, 0.19.

graph is basically a linear cluster state connecting all N qumodes, which were initially forming $N/2$ independent pairs. The state is very similar to the one previously created by interfering 2 independent QOFCs [3].

4. Effect of the modulation index

a. Graph valence. An interesting question is of the effect of the modulation index m on the generated quantum state. Note that the strongest edges in Fig.8 are the former EPR edges. The new edges can therefore be viewed as resulting entirely from the phase modulation. However, this statement cannot be taken literally, as it is crucial to note that the modulation-caused graph edges

link qumodes of very different frequencies, whereas the EOM only couples qumodes separated by 1 FSR.

As m increases, the classical FM spectrum imprinted by the EOM to a single-mode coherent state acquires higher-order sidebands and also sees the carrier amplitude decrease, as illustrated by the insets in Fig.10. Figure 9 shows the evolution of the *trimmed* graph state with m . This shows that phase modulation is a powerful tech-

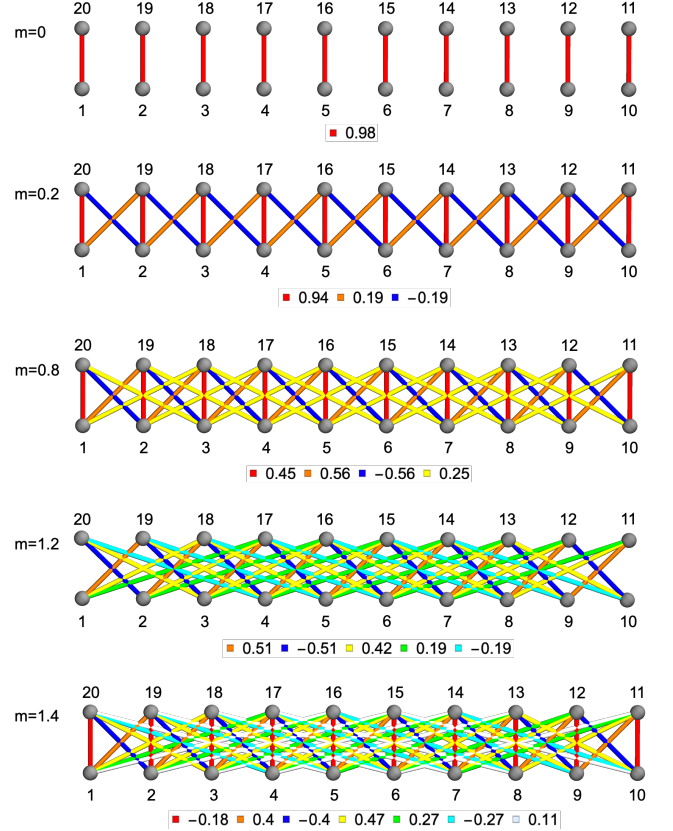


FIG. 9. Trimmed graph of Fig.6, at $\epsilon_{\min} = 0.1$, for different values of m . Note that the EPR edges vanish at $m = 1.2$, before reappearing with opposite weights at $m > 1.2$.

nique for quantum state engineering: applied to a single EPR QOFC, it is able to “knit up” an N -partite linear graph state from $N/2$ initial disjoint EPR qumode pairs, thereby increasing the topological dimension of the graph from zero to one.

Three effects are present: (i), the weights of the initial EPR edges decrease as m increases, going through a zero at $m = 1.2$ before turning negative, (ii), additional edges appear (though, again, *not* between the qumodes coupled by the EOM) and, (iii) the weights of the additional edges increase with m , in the range shown.

The modulation index is therefore a useful parameter to tune the valence of the graph. Even though the trend appears monotonous in the range studied in Fig.9 (more additional edges as m increases), it is reasonable to assume this is, in fact, guided by the classical FM spectrum of Bessel functions (which might explain the zeroing out

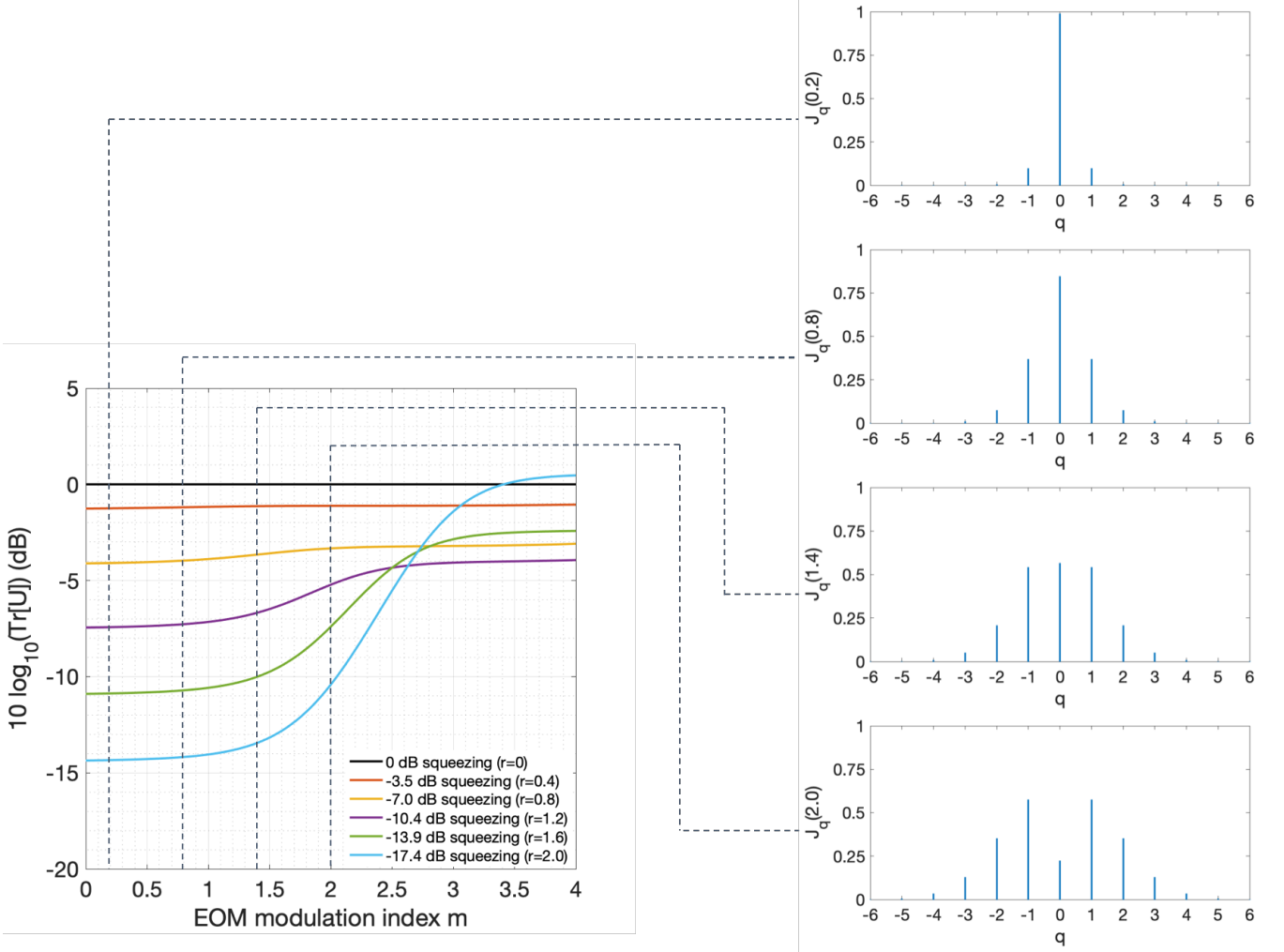


FIG. 10. Dependence of graph error on modulation index m for various squeezing levels. Insets: classical FM spectrum corresponding to the value of m .

of the former EPR edges). In the next section, we'll discuss an additional degree of freedom that can be used as a quantum control parameter in graph state engineering.

b. Graph error. The effect of the modulation index on the graph error \mathbf{U} is a complex question but some measure of physical intuition can be built up by considering, again, the classical phase modulation spectrum, as illustrated in Fig.10.

As is clearly visible, $\text{Tr}[\mathbf{U}]$ remains at the squeezing level for small values of $m < 2$, which means the obtained graph is a valid one. However, this changes dramatically when $m > 2$. Looking at the Bessel function spectra in the insets of Fig.10, we see that, with the modulated carrier going through its first zero, $m \gtrsim 2$ actually corresponds to a physically significant transition from nearest-neighbor coupling to next-neighbor coupling, which is bound to deeply affect the graph structure.

Another important point to consider is that the value of $\text{Tr}[\mathbf{U}]$ does depend critically on the single-mode unitaries, i.e., phase shifts, used to minimize it. When the

graph generation mechanism changes significantly, e.g. $m \gtrsim 2$, then the local constraints toward the minimization of $\text{Tr}[\mathbf{U}]$ change as well.

An extensive study of this situation, in particular of the effect of the squeezing level on the dependence of $\text{Tr}[\mathbf{U}]$ on $m > 2$, is of great interest but well beyond the scope of this paper, in which we limit ourselves to values of $m \lesssim 1$, thereby limiting phase modulation to a single pair of sidebands, i.e., coupling to nearest neighbors only, as depicted in Fig.1(b).

B. Generation of 2D graph states by phase modulation of two interfering QOFCs

We now revisit the configuration used to generate record-scale multipartite linear cluster states in the QOFC [3] by adding phase modulation to the outputs, as depicted in Fig.11. We start from two independent (orthogonally polarized) but frequency-locked EPR QOFCs.

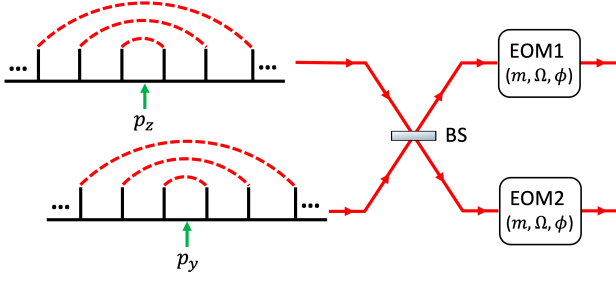


FIG. 11. Phase modulation of two interfering QOFCs. Same conventions as Fig.3.

This can be realized with a single OPO below threshold containing two identical PPKTP crystals quasiphase-matching the ZZZ interaction, oriented at 90° from each other, and pumped by two fields whose frequencies are shifted by 2 OPO FSR [3]. We denote this pump detuning by the variable $\Delta = 2$, in units of the OPO FSR.

The two QOFCs are subsequently interfered with each other at a balanced beamsplitter to generate a dual-rail cluster state [3], as depicted in Fig.12. We then subject

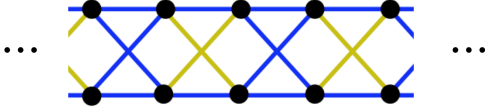


FIG. 12. Linear cluster state obtained by interference of two shifted QOFCs [3].

the output to phase modulation with an EOM in each output port of the beamsplitter. Note that the mirror symmetry present in Section III A with respect to the pump’s half-frequency is absent here, and we will therefore adopt a different pattern for the local phase shifts needed to minimize $\text{Tr}[\mathbf{U}]$: here, we apply a Fourier transform to every other qumode, as frequency ordered.

Remarkably, we can distinguish the two cases of Ω even and odd here, which give different results. Also, $\Omega > 2$ will be a parameter of the final graph structure.

1. Ω odd

We take the particular value $\Omega = 7$ as an illustration in this case. Following the same procedure, we calculate the \mathbf{Z} matrix for the graph and check that $\text{Tr}[\mathbf{U}]$ vanishes before we consider the graph. The graph is displayed in Fig.13 and displays hints of a two-dimensional topological structure.

We now examine the trimmed graph for realistic values of the squeezing parameter. Figure 14 displays the trimmed graph for $\varepsilon_{\min} = 0.1$. The main feature of this graph, which is also one of the main results of this paper, is that it is a square lattice (of width 2Ω), as required for

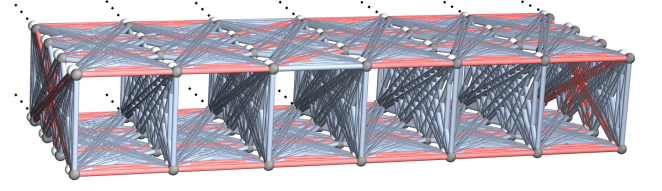


FIG. 13. Graph state for $\Omega = 7$, $m = 0.2$. The red edges denote the “initial” linear cluster state (see Fig.12) created before phase modulation.

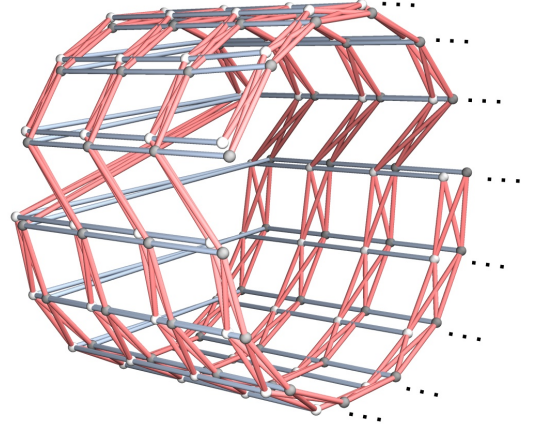


FIG. 14. Trimmed graph state of Fig.13; $\Omega = 7$, $\varepsilon_{\min} = 0.1$. The red edges denote the “initial” linear cluster state (see Fig.12) created before phase modulation.

universal quantum computing. Another crucial point is that, in an analogous manner to the previous case of Section III A, the trimmed graph can be viewed as the initial graph before modulation with additional edges created by phase modulation, albeit not from the literal EOM nearest-neighbor coupling. Note that that initial linear graph is wrapped into a double helix whose circumference has 2Ω qumodes.

2. Ω even

This second case also yields a two-dimensional lattice, although of more intricate structure (which isn’t an obstacle to quantum computing, see for example Ref. 7). The initial and trimmed graphs are displayed in Fig.15. In this case, the initial linear cluster state is “wrapped” into a single spiral whose circumference has Ω qumodes.

Hence, as in Section III A where the phase modulation threaded the zero-dimensional graph of disjoint EPR pairs into a one-dimensional cluster state, here phase modulation applied to an initial linear cluster state weaves it into plane-embedded cluster states which are

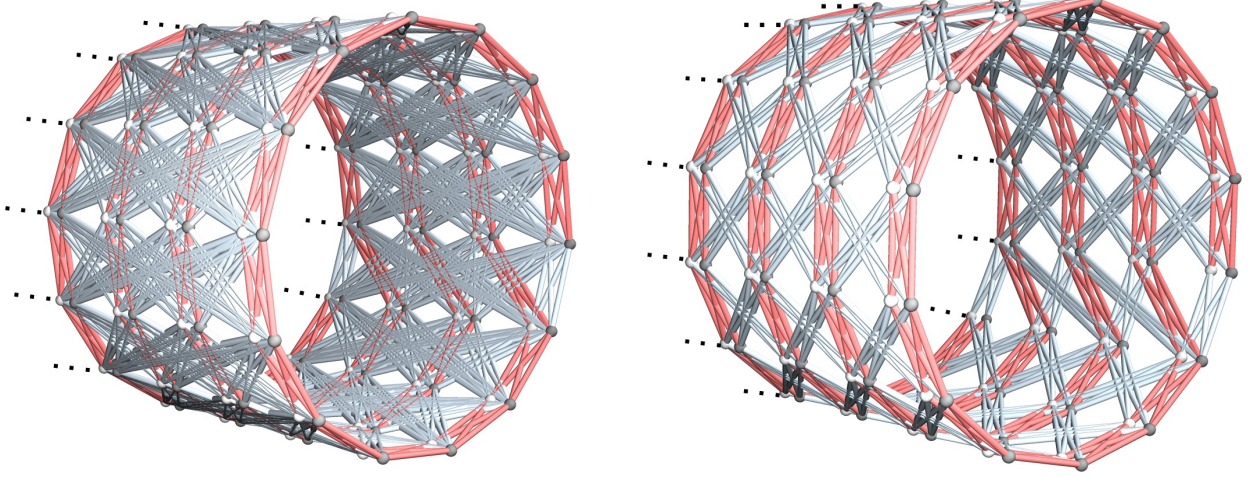


FIG. 15. Left, Initial graph for $\Omega = 14$, $m = 0.2$. Right, Trimmed graph with $\varepsilon_{\min} = 10^{-2}$.

suitable resources for one-way quantum computing.

3. Effect of the coherence of the modulation fields

The relative phase of the RF EOM fields is crucial in the above, as both EOMs are assumed to be modulating in phase. If the relative phase of the RF EOM fields changed, the graphs would change in intricate ways—which will be addressed in detail in a subsequent paper. This effect can, however, be illustrated by a very simple example. Consider the setup of Fig.16, in which two dif-

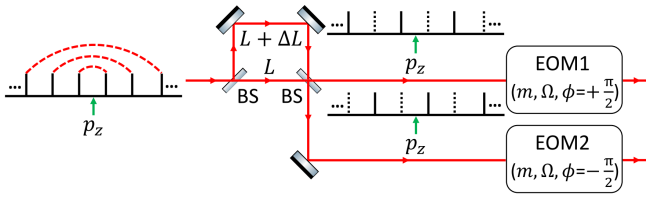


FIG. 16. Modulation of entangled sub-combs. Note that we must have Ω even to prevent vacuum contamination of the sub-combs.

ferent sub-combs of the same initial QOFC are generated such that the EPR correlations straddle the sub-combs, by using a Mach-Zehnder interferometer of path length difference $\Delta L = c/(2\text{FSR})$ to separate out every other frequency.

If the RF fields of the two EOMs are in phase, modulation at, say, $\Omega = 2$ (Ω is required to be even in order to prevent contamination of the sub-comb by vacuum modes) is strictly equivalent to the first case of this paper, Section III A, and will give two 1D graphs similar to Figs.4 & 8, one over the even-frequency sub-comb and one over the odd-frequency sub-comb. However, if the

RF fields of the two EOMs are exactly out of phase and the modulation indices are, of course, identical, one can show that the two phase modulations cancel each other and the resulting graph is identical to the initial one, i.e., independent EPR pairs as in Fig.9, top.

This spectacular effect of the modulation coherence on quantum state engineering is important. A variant of it was observed previously in the different context of tailoring a multitone local oscillator for the homodyne detection of cluster state nullifiers [2]. This destructive interference can be used as a mechanism for controlling the valence of the quantum graph. All too often, quantum graph engineering faces situations where the graphs tend to be completely connected, see Fig.4, Fig.13, or Fig.15. The trimming analysis presented in this paper simplifies them greatly but is only an account of realistic experimental parameters like finite squeezing, not a quantum control technique. The phase coherent modulation of entangled sub-combs can, by way of destructive interference, make an initially high valence graph much sparser and sparse enough graph to be of use for quantum computing [23–25].

IV. CONCLUSION

Phase modulation of the EPR QOFC is a promising, remarkably compact technique for quantum state engineering. It can be used to increase the topological dimension of frequency encoded graph state, solely by phase modulation. Moreover, the modulation parameters, the modulation index, the modulation frequency, and the modulation phase, all have powerful effects on the type of quantum graph that is generated. (Note also that an EOM can be driven by a more complicated RF signal than the monochromatic ones considered in this paper.)

Finally, the conceptual simplicity of this approach makes it well suited for implementations in integrated photonics [34, 35], if loss levels can be kept sufficiently low.

ACKNOWLEDGMENTS

This work was supported by NSF grants PHY-1820882, DMR-1839175, and EECS-1842641, and by BSF grant

2017743.

-
- [1] O. Pfister, Continuous-variable quantum computing in the quantum optical frequency comb, *Journal of Physics B: Atomic, Molecular and Optical Physics* **53**, 012001 (2020).
 - [2] M. Pysher, Y. Miwa, R. Shahrokshahi, R. Bloomer, and O. Pfister, Parallel generation of quadripartite cluster entanglement in the optical frequency comb, *Phys. Rev. Lett.* **107**, 030505 (2011).
 - [3] M. Chen, N. C. Menicucci, and O. Pfister, Experimental realization of multipartite entanglement of 60 modes of a quantum optical frequency comb, *Phys. Rev. Lett.* **112**, 120505 (2014).
 - [4] J. Roslund, R. Medeiros de Araújo, S. Jiang, C. Fabre, and N. Treps, Wavelength-multiplexed quantum networks with ultrafast frequency combs, *Nat. Photon.* **8**, 109 (2014).
 - [5] J.-i. Yoshikawa, S. Yokoyama, T. Kaji, C. Sornphiphatphong, Y. Shiozawa, K. Makino, and A. Furusawa, Invited article: Generation of one-million-mode continuous-variable cluster state by unlimited time-domain multiplexing, *APL Photonics* **1**, 060801 (2016).
 - [6] W. Asavanant, Y. Shiozawa, S. Yokoyama, B. Charoensombutamon, H. Emura, R. N. Alexander, S. Takeda, J.-i. Yoshikawa, N. C. Menicucci, H. Yonezawa, and A. Furusawa, Generation of time-domain-multiplexed two-dimensional cluster state, *Science* **366**, 373 (2019), <https://science.sciencemag.org/content/366/6463/373.full.pdf>
 - [7] M. V. Larsen, X. Guo, C. R. Breum, J. S. Neergaard-Nielsen, and U. L. Andersen, Deterministic generation of a two-dimensional cluster state, *Science* **366**, 369 (2019), <https://science.sciencemag.org/content/366/6463/369.full.pdf>.
 - [8] H. J. Briegel and R. Raussendorf, Persistent entanglement in arrays of interacting particles, *Phys. Rev. Lett.* **86**, 910 (2001).
 - [9] R. Raussendorf and H. J. Briegel, A one-way quantum computer, *Phys. Rev. Lett.* **86**, 5188 (2001).
 - [10] J. Zhang and S. L. Braunstein, Continuous-variable Gaussian analog of cluster states, *Phys. Rev. A* **73**, 032318 (2006).
 - [11] N. C. Menicucci, P. van Loock, M. Gu, C. Weedbrook, T. C. Ralph, and M. A. Nielsen, Universal quantum computation with continuous-variable cluster states, *Phys. Rev. Lett.* **97**, 110501 (2006).
 - [12] J. M. Lukens and P. Lougovski, Frequency-encoded photonic qubits for scalable quantum information processing, *Optica* **4**, 8 (2017).
 - [13] M. Kues, C. Reimer, J. M. Lukens, W. J. Munro, A. M. Weiner, D. J. Moss, and R. Morandotti, Quantum optical microcombs, *Nature Photonics* **13**, 170 (2019).
 - [14] N. C. Menicucci, Fault-tolerant measurement-based quantum computing with continuous-variable cluster states, *Phys. Rev. Lett.* **112**, 120504 (2014).
 - [15] K. Fukui, A. Tomita, A. Okamoto, and K. Fujii, High-threshold fault-tolerant quantum computation with analog quantum error correction, *Phys. Rev. X* **8**, 021054 (2018).
 - [16] M. Pysher, A. Bahabad, P. Peng, A. Arie, and O. Pfister, Quasi-phase-matched concurrent nonlinearities in periodically poled KTiPO₄ for quantum computing over the optical frequency comb, *Opt. Lett.* **35**, 565 (2010).
 - [17] P. Wang, M. Chen, N. C. Menicucci, and O. Pfister, Weaving quantum optical frequency combs into hypercubic cluster states, *Phys. Rev. A* **90**, 032325 (2014).
 - [18] R. N. Alexander, P. Wang, N. Sridhar, M. Chen, O. Pfister, and N. C. Menicucci, One-way quantum computing with arbitrarily large time-frequency continuous-variable cluster states from a single optical parametric oscillator, *Phys. Rev. A* **94**, 032327 (2016).
 - [19] G. Patera, C. Navarrete-Benlloch, G. de Valcárcel, and C. Fabre, Quantum coherent control of highly multipartite continuous-variable entangled states by tailoring parametric interactions, *Eur. Phys. J. D* **66**, 241 (2012).
 - [20] J. Capmany and C. R. Fernández-Pousa, Quantum model for electro-optical phase modulation, *J. Opt. Soc. Am. B* **27**, A119 (2010).
 - [21] M. Hein, J. Eisert, and H. J. Briegel, Multiparty entanglement in graph states, *Phys. Rev. A* **69**, 062311 (2004).
 - [22] M. Gu, C. Weedbrook, N. C. Menicucci, T. C. Ralph, and P. van Loock, Quantum computing with continuous-variable clusters, *Phys. Rev. A* **79**, 062318 (2009).
 - [23] D. Bacon, Too entangled to quantum compute one-way, *Physics* **2**, 38 (2009).
 - [24] D. Gross, S. T. Flammia, and J. Eisert, Most quantum states are too entangled to be useful as computational resources, *Phys. Rev. Lett.* **102**, 190501 (2009).
 - [25] M. J. Bremner, C. Mora, and A. Winter, Are random pure states useful for quantum computation?, *Phys. Rev. Lett.* **102**, 190502 (2009).
 - [26] B. Yurke, Optical back-action-evading amplifiers, *J. Opt. Soc. Am. B* **2**, 732 (1985).
 - [27] In graph theory, an adjacency matrix element $G_{jk} \neq 0$ denotes an edge of weight the element between vertices j and k .
 - [28] N. C. Menicucci, S. T. Flammia, H. Zaidi, and O. Pfister, Ultracompact generation of continuous-variable cluster states, *Phys. Rev. A* **76**, 010302(R) (2007).
 - [29] N. C. Menicucci, S. T. Flammia, and P. van Loock, Graphical calculus for Gaussian pure states, *Phys. Rev.*

- A **83**, 042335 (2011).
- [30] W.-C. Yueh, Eigenvalues of several tridiagonal matrices, *Applied mathematics e-notes* **5**, 210 (2005).
 - [31] P. Wang, W. Fan, and O. Pfister, Engineering large-scale entanglement in the quantum optical frequency comb: influence of the quasiphasematching bandwidth and of dispersion, *arXiv:1403.6631 [physics.optics]* (2014).
 - [32] Z. Y. Ou, S. F. Pereira, H. J. Kimble, and K. C. Peng, Realization of the Einstein-Podolsky-Rosen paradox for continuous variables, *Phys. Rev. Lett.* **68**, 3663 (1992).
 - [33] C. Schori, J. L. Sørensen, and E. S. Polzik, Narrow-band frequency tunable light source of continuous quadrature entanglement, *Phys. Rev. A* **66**, 033802 (2002).
 - [34] F. Lenzini, J. Janousek, O. Thearle, M. Villa, B. Haylock, S. Kasture, L. Cui, H.-P. Phan, D. V. Dao, H. Yonezawa, P. K. Lam, E. H. Huntington, and M. Lobino, Integrated photonic platform for quantum information with continuous variables, *Sci. Adv.* **4**, 10.1126/sciadv.aat9331 (2018), <https://advances.sciencemag.org/content/4/12/eaat9331.full.pdf>.
 - [35] V. D. Vaidya, B. Morrison, L. G. Helt, R. Shahrokhshahi, D. H. Mahler, M. J. Collins, K. Tan, J. Lavoie, A. Reipingon, M. Menotti, N. Quesada, R. C. Pooser, A. E. Lita, T. Gerrits, S. W. Nam, and Z. Vernon, Broad-band quadrature-squeezed vacuum and nonclassical photon number correlations from a nanophotonic device (2019), *arXiv:1904.07833 [quant-ph]*.